

A stochastic spectral analysis of transcriptional regulatory cascades

Aleksandra M. Walczak*

Princeton Center for Theoretical Science, Princeton University, Princeton, NJ 08544

Andrew Mugler†

Department of Physics, Columbia University, New York, NY 10027

Chris H. Wiggins‡

*Department of Applied Physics and Applied Mathematics,
Center for Computational Biology and Bioinformatics, Columbia University, New York, NY 10027*

The past decade has seen great advances in our understanding of the role of noise in gene regulation and the physical limits to signaling in biological networks. Here we introduce the *spectral* method for computation of the joint probability distribution over all species in a biological network. The spectral method exploits the natural eigenfunctions of the master equation of birth-death processes to solve for the joint distribution of modules within the network, which then inform each other and facilitate calculation of the entire joint distribution. We illustrate the method on a ubiquitous case in nature: linear regulatory cascades. The efficiency of the method makes possible numerical optimization of the input and regulatory parameters, revealing design properties of, e.g., the *most informative* cascades. We find, for threshold regulation, that a cascade of strong regulations converts a unimodal input to a bimodal output, that multimodal inputs are no more informative than bimodal inputs, and that a chain of up-regulations outperforms a chain of down-regulations. We anticipate that this numerical approach may be useful for modeling noise in a variety of small network topologies in biology.

Transcriptional regulatory networks are composed of genes and proteins, which are often present in small numbers in the cell [1, 2], rendering deterministic models poor descriptions of the counts of protein molecules observed experimentally [3, 4, 5, 6, 7, 8, 9]. Probabilistic approaches have proven necessary to account fully for the variability of molecule numbers within a homogenous population of cells. A full stochastic description of even a small regulatory network proves quite challenging. Many efforts have been made to refine simulation approaches [10, 11, 12, 13, 14], which are mainly based on the varying step Monte Carlo or ‘Gillespie’ method [15, 16]. Yet expanding full molecular simulations to larger systems and scanning parameter space is computationally expensive. On the other hand the interaction of many protein and gene types makes analytical methods hard to implement. A wide class of approximations to the master equation, which describes the evolution of the probability distribution, focuses on limits of large concentrations or small switches [17, 18, 19]. Approximations based on timescale separation of the steps of small signaling cascades have been successfully used to calculate escape properties [20, 21, 22].

In this paper we introduce a new method for calculating the steady-state distributions of chemical reactants. The procedure, which we call the *spectral method*, relies on exploiting the natural basis of a simpler problem from the same class. The full problem is then solved numerically as an expansion in this basis, reducing the master equation to a set of linear algebraic equations. We break up the problem into two parts: a preprocess-

ing step, which can be solved algorithmically; and the parameter-specific step of obtaining the actual probability distributions. The spectral method allows for huge computational gains with respect to simulations.

We illustrate the spectral method for the case of regulatory cascades: downstream genes responding to concentrations of transcription factors produced by upstream genes which are linked to external cues. Cascades play an important role in a diversity of cellular processes [23, 24, 25], from decision making in development [26] to quorum sensing among cells [27]. We take a coarse-grained approach, modeling each step of a cascade with a general regulatory function that depends on the copy number of the reactant at the previous step (cf. Fig. 1). While the method as implemented describes arbitrary regulation functions, we optimize the information transmission in the case of the most biologically simple regulation function: a discontinuous threshold, in which a species is created at a high or low rate depending on the copy count of the species directly upstream. In the next sections, we outline the spectral method and present in detail our findings regarding signaling cascades.

METHOD

We calculate the steady-state joint distribution for L chemical species in a cascade (cf. Fig. 1). The approach we take involves two key observations: the master equation, being linear,[40] benefits from solution in terms of its eigenfunctions; and the behavior of a given species

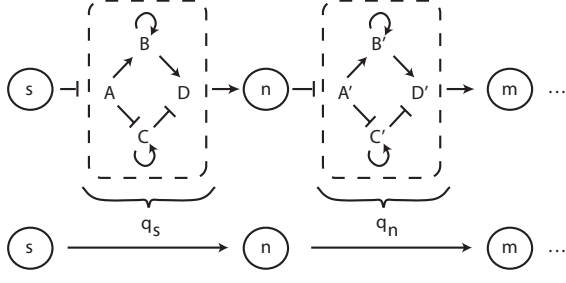


FIG. 1: A schematic representation of a general signaling cascade. Interactions between species of interest may include intermediate processes; we take a coarse-grained approach, condensing these intermediate processes into a single effective regulatory function. For example, the regulatory function q_n describes the creation rate of a species with copy count m as a function of the copy count n of the previous species.

should depend only weakly on distant nodes given the proximal nodes.

The second of these observations can be illustrated succinctly by considering a three-gene cascade in which the first may be eliminated by marginalization. For three species obeying $s \xrightarrow{q_s} n \xrightarrow{q_n} m$ as in Fig. 1, we have the linear master equation

$$\begin{aligned} \dot{p}_{snm} = & \tilde{\rho} [gp_{(s-1)nm} - gp_{snm} + (s+1)p_{(s+1)nm} - sp_{snm}] \\ & + q_s p_{s(n-1)m} - q_s p_{snm} + (n+1)p_{s(n+1)m} - np_{snm} \\ & + \rho [q_n p_{sn(m-1)} - q_n p_{snm} + (m+1)p_{sn(m+1)} - mp_{snm}]. \end{aligned} \quad (1)$$

Here time is rescaled by the first gene's degradation rate, so that each gene's creation rate (g , q_s , or q_n) is normalized by its respective degradation rate; $\tilde{\rho}$ and ρ are the ratios of the first and third gene's degradation rate to the second's, respectively.

To integrate out the first species, we sum over s . We then introduce g_n , the effective regulation of n , by

$$\sum_s q_s p_{nms} = p_{nm} \sum_s q_s p_{s|nm} \approx p_{nm} \sum_s q_s p_{s|n} \equiv g_n p_{nm}. \quad (2)$$

Here we have made the Markovian approximation that s is conditionally independent of m given n . Generally speaking, the probability distribution depends on all steps of the cascade. However since there are no loops in the cascades we consider here, we assume in Eqn. 2 that at steady-state each species is not affected by species two or more steps downstream in the cascade. The validity of the Markovian approximation is tested using both a non-Markovian tensor implementation of the spectral method and a stochastic simulation using the Gillespie algorithm [16], as discussed in *Supplementary Material*. We find that the approximation produces accurate results for all but the most strongly discontinuous regulation functions; even in these cases qualitative features such as modality of the output distribution and locations of the modes are

preserved. Armed with the Markovian approximation the equation for the remaining two species simplifies to

$$\begin{aligned} \dot{p}_{nm} = & g_{n-1} p_{(n-1)m} - g_n p_{nm} + (n+1)p_{(n+1)m} - np_{nm} \\ & + \rho [q_n p_{n(m-1)} - q_n p_{nm} + (m+1)p_{n(m+1)} - mp_{nm}]. \end{aligned} \quad (3)$$

This procedure can be extended indefinitely for a cascade of arbitrary length L , in which modules consisting of pairs of adjacent species are each described by two-dimensional master equations.

The distribution for the first two species is obtained by summing over all other species, which gives an equation of the same form as Eqn. 3 but with $g_n = g = \text{constant}$. If instead the input distribution is an arbitrary p_n , the distribution for the first two species is still described by Eqn. 3, but with g_n calculated recursively from p_n via $g_n = (-np_n + g_{n-1}p_{n-1} + (n+1)p_{n+1})/p_n$ with $g_0 = p_1/p_0$ to initialize.[41] Describing the start of a cascade (with arbitrary input distribution) and describing subsequent steps both amount to solving Eqn. 3 with g_n given by either the recursive equation or Eqn. 2 respectively.

We solve Eqn. 3 by defining the generating function [28] $G(x, y) = \sum_{n,m} p_{nm} x^n y^m$ over complex variables x and y . [42] It will prove more convenient to write the generating function in a state space as $|G\rangle = \sum_{n,m} p_{nm} |n, m\rangle$, [43] with inverse transform $p_{nm} = \langle n, m | G \rangle$, where the states $|i\rangle$ and $\langle i|$, for $i \in \{n, m\}$, along with the inner product $\langle i | i' \rangle = \delta_{ii'}$, define the protein number basis. With these definitions, Eqn. 3 at steady-state becomes $0 = \hat{H} |G\rangle$, where

$$\hat{H} = \hat{b}_n^+ \hat{b}_n^- (n) + \rho \hat{b}_m^+ \hat{b}_m^- (n). \quad (4)$$

Here we have introduced raising and lowering operators in protein space [29, 30, 31, 32] obeying $\hat{b}_i^+ |i\rangle = |i+1\rangle - |i\rangle$ for $i \in \{n, m\}$, $\hat{b}_n^- (n) |n\rangle = n |n-1\rangle - \hat{g}_n |n\rangle$ and $\hat{b}_m^- (n) |n, m\rangle = m |n, m-1\rangle - \hat{q}_n |n, m\rangle$, [44] and the regulation functions have become operators obeying $\hat{g}_n |n\rangle = g_n |n\rangle$ and $\hat{q}_n |n\rangle = q_n |n\rangle$.

Were the operators $\hat{b}_n^- (n)$ and $\hat{b}_m^- (n)$ not n -dependent, \hat{H} would be easily diagonalizable. In fact, this corresponds to the uncoupled case, in which there is no regulation, and both upstream and downstream gene undergo independent birth-death processes with Poisson steady-state distributions. We exploit this fact by working with the respective deviations of g_n and q_n from some constant creation rates \bar{g} and \bar{q} . Then \hat{H} can be partitioned as $\hat{H} = \hat{H}_0 + \hat{H}_1$, where

$$\hat{H}_0 = \hat{b}_n^+ \bar{b}_n^- + \rho \hat{b}_m^+ \bar{b}_m^- \quad (5)$$

$$\hat{H}_1 = \hat{b}_n^+ \hat{\Gamma}_n + \rho \hat{b}_m^+ \hat{\Delta}_n, \quad (6)$$

and we define new operators $\bar{b}_n^- |n\rangle = n |n-1\rangle - \bar{g} |n\rangle$, $\bar{b}_m^- |m\rangle = m |m-1\rangle - \bar{q} |m\rangle$, $\hat{\Gamma}_n = \bar{g} - \hat{g}_n$, and $\hat{\Delta}_n = \bar{q} - \hat{q}_n$. $\hat{\Gamma}_n$ and $\hat{\Delta}_n$ capture the respective deviations of g_n and q_n from \bar{g} and \bar{q} , and \hat{H}_0 is diagonal in the eigenbases $|j\rangle$ and

$|k\rangle$ of the uncoupled birth-death processes at rates \bar{g} and \bar{q} respectively;[45] specifically $\hat{H}_0|j, k\rangle = (j + \rho k)|j, k\rangle$. Projecting Eqn. 4 onto the eigenbasis yields the linear equation of motion

$$(j + \rho k)G^{jk} + \sum_{j'} \Gamma_{j-1, j'} G^{j'k} + \rho \sum_{j'} \Delta_{jj'} G^{j', k-1} = 0, \quad (7)$$

where $G^{jk} = \langle j, k|G\rangle$, $\Gamma_{jj'} = \sum_n (\bar{g} - g_n) \langle j|n\rangle \langle n|j'\rangle$, and $\Delta_{jj'} = \sum_n (\bar{q} - q_n) \langle j|n\rangle \langle n|j'\rangle$. Eqn. 7 exploits the subdiagonal nature of the k -dependence; it is initialized using $G^{j0} = \sum_n p_n \langle j|n\rangle$, then solved exactly by matrix inversion for each subsequent k . The joint distribution is retrieved via the inverse transform as

$$p_{nm} = \sum_{jk} \langle n|j\rangle G^{jk} \langle m|k\rangle. \quad (8)$$

One computational advantage is that the overlap integrals $\langle n|j\rangle$ and $\langle j|n\rangle$ need only be evaluated explicitly for $\langle n|j=0\rangle = e^{-\bar{g}} \bar{g}^n/n!$ and $\langle j|n=0\rangle = (-\bar{g})^j/j!$; all other values can be obtained recursively using the selection rules $\langle n|j+1\rangle = \langle n-1|j\rangle - \langle n|j\rangle$ and $\langle j|n+1\rangle = \langle j-1|n\rangle + \langle j|n\rangle$. [46] The same holds for $\langle m|k\rangle$, taking $n \rightarrow m$, $j \rightarrow k$, and $\bar{g} \rightarrow \bar{q}$. Note that once \bar{g} and \bar{q} have been chosen, [47] the calculation can be separated into a preprocessing step, in which the matrices $\langle n|j\rangle$, $\langle j|n\rangle$, and $\langle m|k\rangle$ are calculated (and potentially reused at subsequent steps of the cascade or for subsequent steps in an optimization), and the actual step of calculating G^{jk} via Eqn. 7.

By exploiting the basis of the uncoupled system, we have reduced Eqn. 3 to a set of simple linear algebraic equations, [48] Eqn. 7, which dramatically speeds up the calculation without sacrificing accuracy (cf. *Results* and *Supplementary Material*). The method is applicable for any input function g_n and regulation function q_n . Solutions using other bases and further generalizations to systems with feedback will be discussed in future work.

RESULTS

The spectral method is fast and accurate

To demonstrate [49] the accuracy and computational efficiency of the spectral method, we compare it both to an iterative numerical solution of Eqn. 3 and to a stochastic simulation using the ‘Gillespie’ algorithm [16] for a cascade of length $L = 2$ with a Poisson input ($g_n = g = \text{constant}$) and the discontinuous threshold regulation function

$$q_n = \begin{cases} q_- & \text{for } n \leq n_0 \\ q_+ & \text{for } n > n_0. \end{cases} \quad (9)$$

The spectral method achieves an agreement up to machine precision with the iterative method in $\sim 0.01s$,

which is ~ 1000 times faster than the iterative method’s runtime and $\sim 10^8$ faster than the runtime necessary for the stochastic simulation to achieve the same accuracy; see *Supplementary Materials* for details. The huge gain in computational efficiency over both the iterative method and the stochastic simulation makes the spectral method extremely useful, particularly for optimization problems, in which the probability function must be evaluated multiple times. In the next sections we exploit this feature to optimize information transmission in signaling cascades.

Information processing in signaling cascades

Linear signaling cascades are a ubiquitous feature of biological networks, used to transmit relevant information from one part of a cellular system to another [23, 24, 25, 26, 27]. Information processing in a cascade is quantified by the mutual information [33], which measures in bits how much information about an input signal is transmitted to the output signal in a noisy process. For a cascade of length L , the mutual information between an input species (with copy number n_1) and an output species (with copy number n_L) [50] is $I = \sum_{n_1, n_L} p(n_1, n_L) \log_2 [p(n_1, n_L)/p(n_1)p(n_L)]$. In this study we define the capacity I^* as the maximum mutual information over either regulatory parameters, the input distribution, or both. Depending on the signal to noise ratio, a high-capacity cascade functions either where the input signal is strongest or where the transmission process is least noisy [34, 35].

We first consider a cascade of length L in which the regulation function q_n is a simple threshold (Eqn. 9) with fixed parameters that are identical for each cascade step. It is worth noting that while a threshold-regulated creation rate represents the simplest choice biologically, it is the most taxing choice computationally: as the discontinuity $\Delta = |q_+ - q_-|$ increases, we find both that (a) a larger cutoff K in eigenmodes is required for a desired accuracy, and (b) the accuracy of the Markovian approximation decreases (cf. *Supplementary Material*). The results herein therefore constitute a stringent numerical challenge for the spectral method.

We take the input $p(n_1)$ to be a Poisson distribution (i.e. $g_n = g = \text{constant}$). In the extreme cases, when the threshold is infinite or zero, the output is a Poisson distribution centered at q_- or q_+ , respectively. Similarly, when the input median is below or above threshold, the output mean should be biased toward q_- or q_+ , respectively. For example, in Fig. 2A, $\langle n_1 \rangle < n_0$, and the output distribution is shifted toward q_- . This effect is amplified at each step of the cascade, such that $\langle n_L \rangle \rightarrow q_-$ for large L . Similarly, $\langle n_L \rangle \rightarrow q_+$ for large L when $\langle n_1 \rangle > n_0$ (Fig. 2C). When $\langle n_1 \rangle \sim n_0$ (Fig. 2B), the output is balanced between q_- and q_+ ; if the discontinuity $\Delta = |q_+ - q_-|$ is sufficiently large, the output is bimodal, as discussed in

more detail in the next section.

Mutual information I decreases monotonically with L for all $\langle n_1 \rangle$ (cf. Fig. 2F), as required by the data processing inequality [36] (i.e. one cannot learn more information from the output of an $(L+1)$ -gene cascade than one could from an L -gene cascade with identical regulation, only less). I is maximal for $\langle n_1 \rangle \sim n_0$ which makes intuitive sense, as it corresponds to the input taking advantage of both rates q_- and q_+ roughly equally in producing the output. A simple calculation quantifies this intuition. Approximating the steady-state distribution for the moment as a strict switch conditional on n_0 (i.e. $p(n_L|n_1) = p_-(n_L)$ if $n_1 < n_0$ and $p(n_L|n_1) = p_+(n_L)$ if $n_1 \geq n_0$ for some distributions $p_{\pm}(n_L)$), it follows from the definition of I that

$$I_{\text{switch}} = S - \sum_{\pm} \sum_{n_L} p_{\pm}(n_L) \log_2 \left[1 + \frac{\pi_{\mp} p_{\mp}(n_L)}{\pi_{\pm} p_{\pm}(n_L)} \right], \quad (10)$$

where $S = -\sum_{\pm} \pi_{\pm} \log_2 \pi_{\pm}$, $\pi_- = \sum_{n_1 < n_0} p(n_1)$ and $\pi_+ = \sum_{n_1 \geq n_0} p(n_1) = 1 - \pi_-$. If there is little overlap between $p_-(n_L)$ and $p_+(n_L)$, then $I_{\text{switch}} \sim S$, which is maximal when $\pi_- = \pi_+$, i.e. when the median of the input distribution $p(n_1)$ lies at the threshold n_0 . Additionally, since the maximal value of S (and I_{switch} , since the summand of the second term in Eqn. 10 is always nonnegative) is 1 bit, this calculation also suggests that the capacity of threshold regulation (in the limit of strict switch-like behavior) is limited to 1 bit. Again, this result is intuitive, as the cascade is only passing on the binary information of whether particles in the input distribution are below or above the threshold.

In an experimental setup one might have access to only the mean response (or “transfer function”), or the variance in response across cells (or “noise”), of a signaling cascade to its input. Since our method yields the full distributions, such summary statistics are readily computed. Despite the sharpness of threshold regulation, the transfer functions are quite smooth even at $L = 2$ (cf. Fig. 2D). The effect of the intrinsic noise is to smooth out a sharp discontinuity in creation rates, producing a continuous mean response. The transfer functions shown are least-squares fit to Hill functions of the form $\langle n_L | n_1 \rangle = \alpha_- + (\alpha_+ - \alpha_-)(n_1)^h / [(n_1)^h + (k_d)^h]$. As one would expect, for all L , best fit values of α_- , α_+ are near the rates q_- and q_+ respectively, and best fit k_d values are near the threshold n_0 . As L increases, the transfer function sharpens, and cooperativity h increases (cf. inset in D), due to the amplified migration of the output to either q_- and q_+ in longer cascades (as in Figs. 2A and 2C).

The strength of the noise increases with L (cf. Fig. 2E), consistent with the reduction in I with L (cf. Fig. 2F), and the noise is peaked at the threshold. The “switch approximation” (cf. Eqn. 10) illustrates the gain in information when the median of the input coincides with the

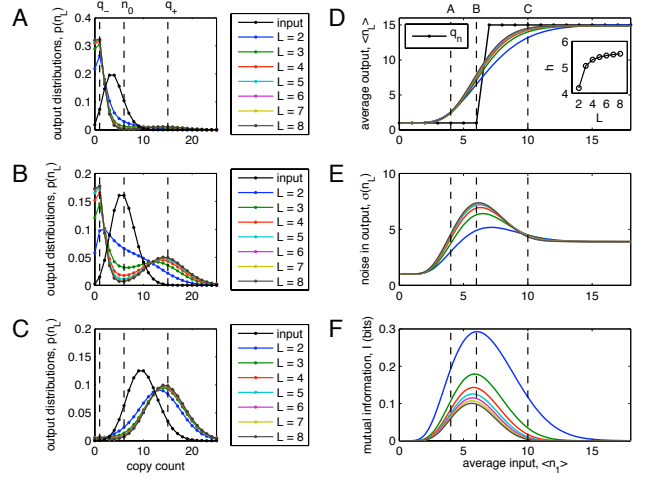


FIG. 2: Transfer functions and noise in a signaling cascade. **A-C:** Plots of input distribution $p(n_1)$ (black) and output distributions $p(n_L)$ (colors; see legend) for various cascade lengths L . Input distribution is a Poisson centered at $\langle n_1 \rangle = 4$ (in A), $\langle n_1 \rangle = n_0 = 6$ (in B), or $\langle n_1 \rangle = 10$ (in C). The regulation function q_n for all steps is a threshold (Eqn. 9) shown in D (black line with dots), with parameters q_- , q_+ , and n_0 overlaid as dashed lines in A-C. The degradation rate ratio is $\rho = 1$, and Eqn. 3 is solved using the spectral method with $\bar{q} = 10$ and $\bar{g} = \langle g_n \rangle$ for each step in the cascade. **D-F:** Transfer functions (average output $\langle n_L \rangle$) (D), noise (standard deviation of the output $\sigma(n_L)$) (E), and mutual information I (F) as functions of average input $\langle n_1 \rangle$ for various cascade lengths L (colors as in A-C). As in A-C, input is Poisson at every $\langle n_1 \rangle$; dashed lines correspond to the specific $\langle n_1 \rangle$ values in A, B, and C. **Inset in D:** Cooperativity h as a function of L .

threshold; the “small noise approximation” [34, 35], however, illustrates the loss in information when the peak of the input coincides with the peak of the noise. The trade-off between these two trends thwarts information transmission with unimodal input distributions (e.g., those used in Fig. 2) and suggests an input distribution with two or more modes should be able to transduce more information. Such distributions are the subject of study below, and, in related work [35, 37] are shown to be the optimal strategy and to be observed in biology for a regulatory system in which peak noise and threshold coincide.

Bimodal output from a unimodal input

A striking feature of Fig. 2B is that the unimodal input is converted to a bimodal output for cascades of length $L = 3$ or longer. Bimodality can arise from a system with two genes whose proteins repress each other or from a single gene whose proteins activate its own expression. Here we demonstrate that cascades with sufficiently strong regulation constitute an information-optimal mechanism

for a cell to achieve bimodality.

Recall that Fig. 2B corresponds to the case where the input distribution is optimally matched with the regulation function, i.e. the bimodal output represents optimal information transmission. By optimizing over the mean g of a Poisson input distribution, we find that the most informative output distribution in a cascade with unimodal input can be unimodal or bimodal, depending on regulatory parameters and the length of the cascade. Fig. 3A shows examples of regulation functions which produce output distributions that are unimodal, bimodal for cascades as long or longer than some L^* (which we term “persistent” bimodality), and bimodal for short cascades but unimodal at both initial and final nodes for longer cascades (which we term “localized” bimodality).

Bimodality is found both in cascades in which each step is down-regulating, which we call “AC” cascades, and in those in which each step is up-regulating, which we call “DC” cascades. In DC cascades, as seen in the insets of panels 1-3 in Fig. 3A, the average output either monotonically decreases or monotonically increases with L . In the former case, since $q_- < n_0$, the probability that the output is below the threshold given that the input is below threshold is large. Successive such regulations drive the probability of being below the threshold towards 1, successively decreasing $\langle n \rangle$ at each step in the cascade. In the latter case, since $q_+ > n_0$, the same picture holds, and $\langle n \rangle$ monotonically increases with L . Whether the monotonically increasing or decreasing behavior is the more informative is determined by the relationship among q_+ , q_- , and n_0 . In AC cascades, an analogous picture holds but with alternation: $\pi_- < \pi_+$ for the even-numbered links (cf. Eqn. 10), and the AC condition $q_- > q_+$ leads to $\pi_+ < \pi_-$ for the odd-numbered links, as illustrated in the insets of panels 4-6 in Fig 3A. These behaviors motivate the names “AC” and “DC,” analogous to alternating and direct current flow. Performance of AC and DC cascades is compared in more detail in the next section.

Fig. 3B shows a phase diagram of optimal output modality as a function of the rates q_- and q_+ : bimodality is found at high values of the discontinuity $\Delta = |q_+ - q_-|$ (specifically, for $\Delta \gtrsim 11$ in AC circuits and $\Delta \gtrsim 12$ in DC circuits when $n_0 = 8$). Intuitively, since the weight of the output is distributed between q_- and q_+ for long cascades, increasing their separation spreads the weights apart and creates bimodal distributions. Furthermore, as Δ increases, the bimodality becomes more robust: it goes from localized to persistent, and its onset occurs at a smaller cascade length L^* . The inset of Fig. 3B shows that capacity I^* also increases with Δ ; cascades with bimodal output therefore have higher capacities than those with unimodal output. As Δ increases, the information transmission properties of a regulatory cascade are better approximated by simple switch-like regulation (cf. Eqn. 10). In short, summarizing the input distribution by π_+

and π_- is a more informative summary of the distribution as the regulation becomes more discontinuous.

Channel capacity in AC/DC cascades

Our setup provides a way to ask quantitatively whether a cascade with down-regulating steps (AC) can transmit information with more or less fidelity than a cascade with down-regulating steps (DC). Since a cell must expend time and energy to make proteins, a fair comparison between cascade types can only be made when the species involved in each type are present in equal copy number. As in [38], we introduce the objective function $L = I - \lambda \langle n \rangle$ where I is mutual information and $\langle n \rangle = \sum_{\ell=1}^L \langle n_\ell \rangle / L$ is an average copy count over all species in the cascade. Here λ represents the metabolic cost of making proteins, and optimizing L for different values of λ allows a comparison of AC and DC capacities I^* at similar values of $\langle n \rangle$.

For both AC and DC cascades, I^* increases with $\langle n \rangle$ as more proteins are made available to encode the signal,[51] and I^* decreases[52] with L at all $\langle n \rangle$ (cf. Fig. 4A). Both AC and DC capacities converge to an L -dependent asymptotic value at high copy count, but DC cascades attain higher capacities per output protein than AC cascades. The difference is most pronounced at low copy count ($\langle n \rangle \lesssim 7$), and more pronounced still for longer cascades. The difference is easily explained: AC and DC cascades of the same length with the same discontinuity $\Delta = |q_+ - q_-|$ have the same capacity but have different mean numbers of proteins. Recall from Fig. 3B that large Δ leads to high-capacity, bimodal solutions. The difference between AC and DC cascades is in the placement of their optimal distributions for a given Δ . We observe that optimal AC cascades tend to exhibit $\langle n \rangle \gtrsim n_0$, while optimal DC cascades tend to exhibit $\langle n \rangle \lesssim n_0$. Ultimately, this allows DC cascades to achieve the same capacity for the same regulation parameters (cf. Fig. 3B inset), but use fewer proteins. These results suggest that DC cascades transmit with higher fidelity per protein than AC cascades when protein production is costly.

The most informative input to a threshold is bimodal

If the first species is governed by more than a simple birth-death process, the input to a cascade will not be a simple Poisson distribution. To investigate the role of input multimodality in information transmission, we consider inputs defined by a mixture of Poisson distributions, $p(n_1) = \sum_{i=1}^Z \pi_i e^{-g_i} g_i^{n_1} / n_1!$, (with $\sum_{i=1}^Z \pi_i = 1$). As before, we expect information to increase with copy

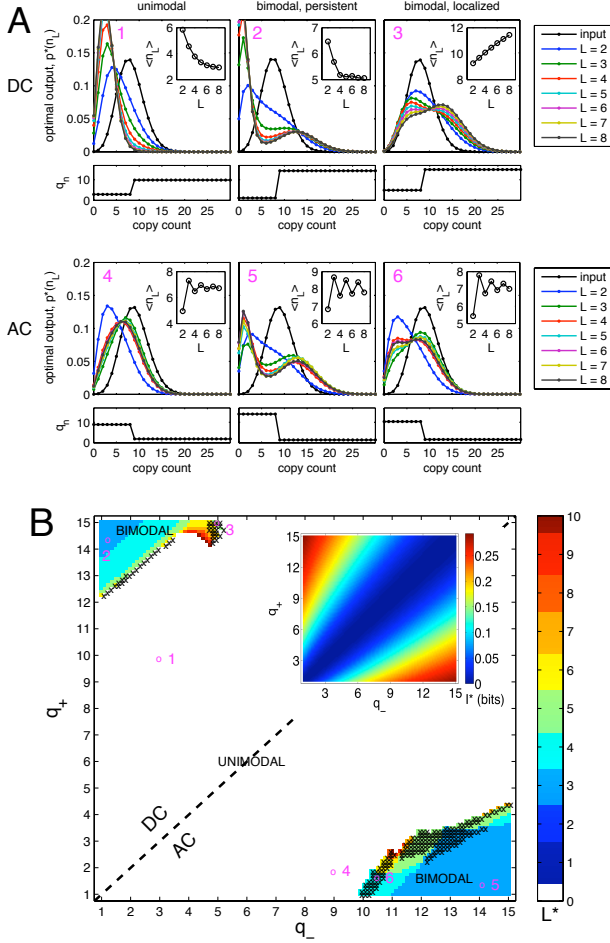


FIG. 3: Optimal output modality in cascades with unimodal input. **A:** Plots of optimal input distribution $p^*(n_1)$ (black) and optimal output distributions $p^*(n_L)$ (colors; see legend) for different cascade lengths L (optimal input distributions are qualitatively the same; only that for $L = 2$ is shown), corresponding to regulation functions q_n (identical for each step) plotted underneath ($\rho = 1$, and solutions used $\bar{q} = 10$ and $\bar{g} = \langle g_n \rangle$). Mutual information I is optimized as a function of the mean g of the Poisson input distribution. Magenta numbers on plots correspond to magenta points in B. Insets show plots of average output $\langle n_L \rangle$ vs. cascade length L . In the first column of A, the output is always unimodal; in the second column, the output is bimodal for cascade lengths $L \geq L^*$ for some L^* (“persistent” bimodality); in the third column, the output is bimodal for a range of L values, then unimodal once more for large L (“localized” bimodality). The first row shows “DC” cascades, in which each step is up-regulating, and the second row shows “AC” cascades, in which each step is down-regulating. **B:** Phase diagram of optimal output modality as a function of q_- and q_+ ($n_0 = 8$). White is unimodal, and color is bimodal, with color corresponding to L^* . Distinction between persistent (no ‘x’) and localized (‘x’) bimodality is shown up to $L = 10$. Dashed line separates DC cascades from AC cascades. **Inset:** Capacity I^* in bits as a function of q_- and q_+ for the same data.

number, and we use the objective function \mathbb{L} when optimizing over the input distribution $p(n_1)$.

All optimal input distributions with $Z \geq 2$ are bimodal, with one mode on either side of the threshold (cf. Fig. 4B). When Z is 3 or more, either all but two π_i values are driven by the optimization to 0, or all the g_i values with nonzero weights are driven to one of two unique values. The two modes are roughly equally weighted (i.e. $\pi_1 \approx \pi_2 \approx 0.5$), consistent once more with our calculation that the median of the optimal input distribution falls roughly at the threshold (cf. Eqn. 10). As an additional verification, a plot of capacity I^* vs. Z in the inset of Fig. 4B reveals that I^* remains constant for $Z = 2$ and beyond. A threshold regulation function presents a binary choice, and the optimal input is a bimodal distribution that equally utilizes both sides. Lastly, we point out that the capacities in the inset of Fig. 4B are below 1 bit. Even with a bimodal input distribution, a short cascade ($L = 2$), and strong regulation functions (i.e. large discontinuities Δ), we do not find capacities above 1 bit. This is consistent with our calculation under the approximation of threshold regulation as a switch (cf. Eqn. 10) and with the intuition that a threshold represents a binary decision.

CONCLUSIONS

We have introduced a method, the *spectral* method, which exploits the linear algebraic structure of the master equation, and expands the full problem in terms of its natural eigenfunctions. We have illustrated our method by probing the optimal transmission properties of signaling cascades with threshold regulation. We have shown that sufficiently long cascades with sufficiently strong regulation functions optimally convert a unimodal input to a bimodal output. A bimodal input is optimal for information transmission across a threshold, and a multimodal input offers no further processing power. Sustained bimodality of the input distribution requires large discontinuities Δ between the production rates below and above the threshold. The value of Δ controls the maximum information transmitted by a cascade with threshold regulation in a similar way for cascades of up-regulations (DC) and cascades of down-regulations (AC), but a DC cascade outperforms an AC cascade by using fewer average copies of its species. We emphasize that the application of the spectral method to signaling cascades represents only a beginning. Variations on the natural bases in which to expand, and extensions of the method to other small network topologies, will be the subject of future work. More generally, however, we anticipate that the method will prove useful in the direct solution of a large class of master equations describing a wide variety of biological systems.

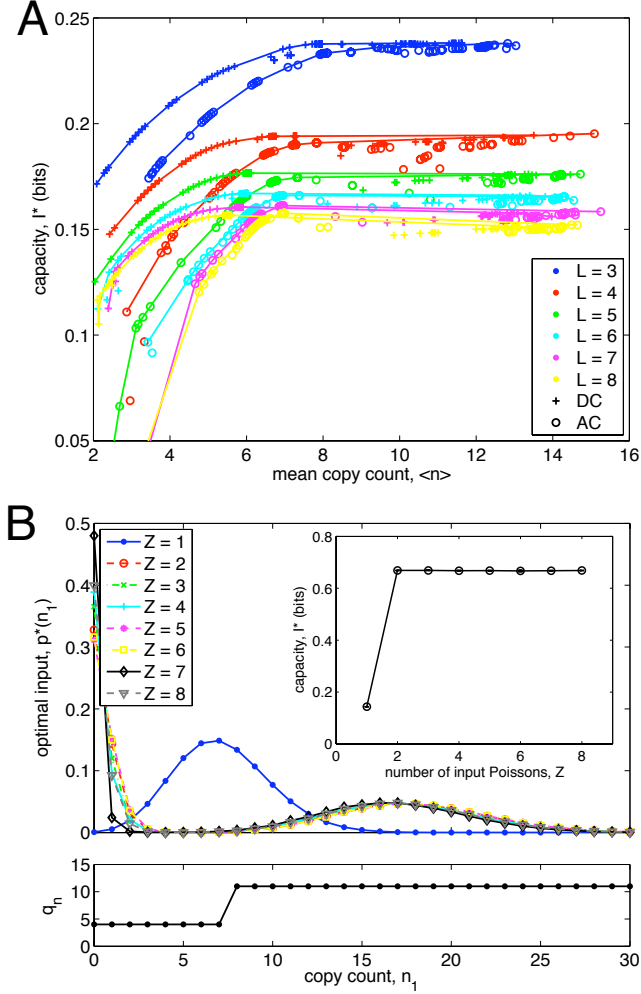


FIG. 4: **A:** Capacities of AC and DC cascades. Capacity I^* vs. average copy count $\langle n \rangle$ (over all species) for AC (circles) and DC (plus signs) cascades of different lengths L (color), with Poisson input distributions. Results were obtained by optimizing the objective function L over all parameters (q_- , q_+ , n_0 , and g) for $\lambda = 1 \times 10^{-6} - 3 \times 10^{-2}$ (n_0 is constrained to be an integer, the regulation function is the same for every step, $\rho = 1$, and solutions used $\bar{q} = 10$ and $\bar{g} = \langle g_n \rangle$). Lines show convex hulls. **B:** Optimal input distributions with different numbers Z of Poisson distributions. The cascade length is $L = 2$, the degradation rate ratio is $\rho = 1$, and the regulation function q_n is plotted in the bottom panel; solutions used $\bar{q} = 10$ and $\bar{g} = \langle g_n \rangle$. The objective function L is optimized with $\lambda = 10^{-4}$ over all input parameters g_i and π_i . **Inset** Capacity I^* vs. Z , averaged at each Z over 7 optimizations with different initial conditions.

SUPPLEMENTARY MATERIAL

The spectral method is fast and accurate

To demonstrate the accuracy and computational efficiency of the spectral method, we compare it both to

an iterative numerical solution and to a stochastic simulation (using the varying step Monte Carlo or ‘Gillespie’ method [15, 16]) of Eqn. 3. Fig. 5A shows the agreement among output distributions p_m generated by the three methods for a cascade of length $L = 2$ with a Poisson input ($g_n = g = \text{constant}$) and the threshold regulation function in Eqn. 9. The spectral method achieves accuracy up to machine precision in ~ 0.01 s, which is ~ 1000 times faster than the iterative method’s runtime and $\sim 10^8$ faster than the runtime necessary for the stochastic simulation to achieve the same accuracy (cf. Fig. 5B). As a measure of error we use the Jensen-Shannon divergence [39] (a measure in bits between two probability distributions) between the distribution p_{nm} generated by the iterative method and that generated by either the spectral method or the stochastic simulation. We plot this measure against the runtime of either method, scaled by the runtime of the iterative method, in Fig. 5B.

Validity of the Markovian approximation

For a cascade of length L , we reduce an L -dimensional master equation to a set of 2-dimensional equations by employing the Markov approximation, i.e. that each species is conditionally independent of distant nodes given proximal nodes (cf. main text). Here we compare results under this approximation with those from a solution of the full master equation, using both a stochastic simulation [16] and a non-Markovian implementation of the spectral method.

The non-Markovian spectral method is implemented as follows. The full master equation for the process $n_1 \xrightarrow{q_2(n_1)} n_2 \xrightarrow{q_3(n_2)} \dots \xrightarrow{q_L(n_{L-1})} n_L$ is

$$\begin{aligned} \dot{p}(\vec{n}) = & gp(\vec{n} - \hat{e}_1) - gp(\vec{n}) + (n_1 + 1)p(\vec{n} + \hat{e}_1) - n_1 p(\vec{n}) \\ & + \sum_{\ell=2}^L \rho_\ell [q_\ell(n_{\ell-1})p(\vec{n} - \hat{e}_\ell) - q_\ell(n_{\ell-1})p(\vec{n}) \\ & + (n_\ell + 1)p(\vec{n} + \hat{e}_\ell) - n_\ell p(\vec{n})], \end{aligned} \quad (11)$$

where time is rescaled by the degradation rate of the first species, g is the creation rate of the first species, q_ℓ is the creation rate of the ℓ th species, creation rates are normalized by corresponding degradation rates, ρ_ℓ is the ratio of the degradation rate of the ℓ th species to that of the first, $\vec{n} = (n_1, \dots, n_L)$, and \hat{e}_ℓ represents a 1 in n_ℓ th direction. Denoting $|j_1, \dots, j_L\rangle$ as the eigenstate of species \vec{n} at constant rates $g, \bar{q}_2, \dots, \bar{q}_L$ respectively, Eqn.

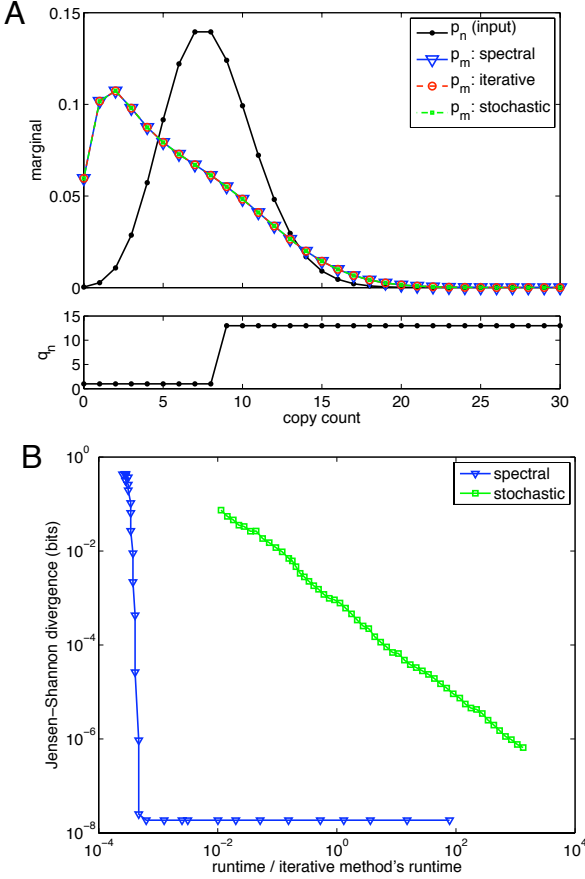


FIG. 5: Demonstration of the spectral method's accuracy and efficiency. **A:** Output distributions p_m obtained by solving Eqn. 3 with $g_n = g = \text{constant}$ using the spectral method described in the main text (blue triangles), an iterative numerical method (red circles), and a stochastic simulation [16] (green squares). Also shown is the input p_n (a Poisson distribution with mean $g = 8$), and the regulation function q_n (Eqn. 9) with $q_- = 1$, $q_+ = 13$, and $n_0 = 8$; the degradation rate ratio is $\rho = 1$. Spectral solution used $\bar{q} = 10$ and mode number cutoffs $J = K = 50$, and all solutions used copy count cutoffs $N = M = 50$. **B:** Jensen-Shannon divergence [39] between p_{nm} obtained using the iterative numerical method and that obtained using the spectral method (blue triangles) or stochastic simulation (green squares), plotted against the latter two methods' respective runtimes. Runtimes are scaled by iterative method's runtime, 15.9 s. Spectral method data obtained by varying K from 3 to 12,589; plateau begins at $K \approx 50$. Stochastic simulation data obtained by varying integration time from 100 to 2×10^7 , in units of the upstream gene's reciprocal degradation rate.

(11) has the spectral decomposition

$$0 = \left(j_1 + \sum_{\ell=2}^L \rho_\ell j_\ell \right) G^{j_1, \dots, j_L} + \sum_{\ell=2}^L \rho_\ell \sum_{j'_{\ell-1}} \Delta_{j_{\ell-1}, j'_{\ell-1}} G^{j_1, \dots, j'_{\ell-1}, j_\ell-1, \dots, j_L}, \quad (12)$$

where $G^{j_1, \dots, j_L} = \langle j_1, \dots, j_L | G \rangle$ and the deviation operator $\Delta_{j_{\ell-1}, j'_{\ell-1}} = \sum_{n_{\ell-1}} [\bar{q}_\ell - q_\ell(n_{\ell-1})] \langle j_{\ell-1} | n_{\ell-1} \rangle \langle n_{\ell-1} | j'_{\ell-1} \rangle$. Eqn. (12) is solved by iteration, initialized with $G^{j_1, \dots, j_L} = \delta_{j_1, 0} \dots \delta_{j_L, 0}$. The joint distribution is obtained via inverse transform:

$$p(n_1, \dots, n_L) = \sum_{j_1, \dots, j_L} \langle n_1 | j_1 \rangle \dots \langle n_L | j_L \rangle G^{j_1, \dots, j_L}. \quad (13)$$

For a cascade of length $L = 4$, with two different values of the discontinuity $\Delta = |q_+ - q_-|$ (cf. Eqn. 9), Figure 6 compares the marginal distributions calculated under the Markov approximation (using both the spectral method and an iterative numerical solution) with those calculated from the full master equation (using both the non-Markovian spectral method and a stochastic simulation). When Δ is small there is full agreement between the Markovian and non-Markovian distributions (cf. Fig. 6A, with $\Delta = 4.5$); as Δ grows, the Markovian distributions begin to deviate from the non-Markovian distributions (cf. Fig. 6B, with $\Delta = 8.5$). The deviation is more pronounced at higher ℓ , i.e. for species more downstream in the cascade. We emphasize, however, that important qualitative features of the distributions, such as modality and locations of the modes, are retained under the approximation.

A note on degradation rates

The ratio ρ of a downstream gene's degradation rate to that of an upstream gene is fixed to 1 in all results in the main text. Increasing ρ is a computationally straightforward way to obtain, e.g., a bimodal output, since it corresponds to the case in which the downstream gene equilibrates more quickly than the upstream gene, such that the output is simply a weighted sum of distributions peaked at each of the threshold values q_- and q_+ (cf. Eqn. 9). Specifically, in the $\rho \rightarrow \infty$ limit, for the two-gene cascade $n \xrightarrow{q_n} m$, $p_m = \pi_- e^{-q_-} q_-^m / m! + \pi_+ e^{-q_+} q_+^m / m!$, where $\pi_- = \sum_{n \leq n_0} p_n$ and $\pi_+ = \sum_{n > n_0} p_n$. However most degradation rates are dominated by cell division, so degradation rate ratios far from than ~ 1 are unrealistic. Our results demonstrate that even with all species operating on the same timescale, relatively short cascades with strong enough regulation provide a information-optimal mechanism of converting a unimodal signal to a bimodal signal.

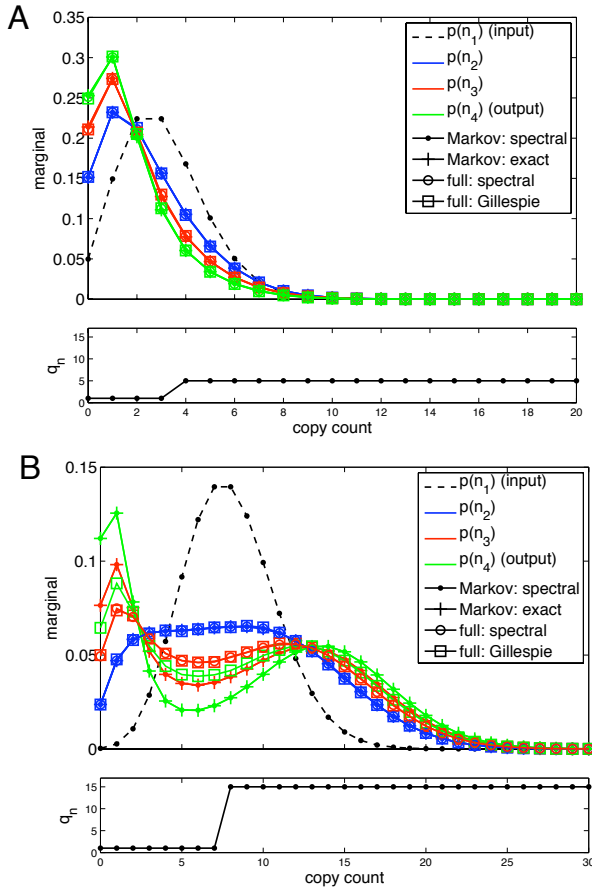


FIG. 6: Marginal distributions from a Markovian and a non-Markovian stochastic description of a cascade. **A:** Marginal distributions for the species in a cascade of length $L = 4$ (colors indicate order of species in the cascade; see legend), with threshold regulation function q_n shown in the bottom panel ($q_- = 0.5$, $q_+ = 5$, and $n_0 = 7$). Distributions were obtained using the Markov approximation (cf. main text), either via the spectral method (dots) or via an iterative numerical solution (plus signs), and using the full master equation (Eqn. 11), either via the non-Markovian spectral method (circles) or via stochastic simulation [16] (squares). **B:** As A, but with $q_+ = 9$.

It is a pleasure to acknowledge Jake Hofman and Melanie Lee for their help in this project. C.W. was supported by NIH 5PN2EY016586-03 and NIH 1U54CA121852-01A1; C.W. and A.M. were supported by NSF ECS-0332479; A.M. was supported by NSF DGE-0742450.

* awalczak@princeton.edu

† ajm2121@columbia.edu

‡ chris.wiggins@columbia.edu

[1] Hooshangi, S, Thiberge, S, Weiss, R (2005) Ultrasensitivity and noise propagation in a synthetic transcriptional

cascade. *Proc Natl Acad Sci USA* 102:3581–6.

[2] Thattai, M, van Oudenaarden, A (2002) Attenuation of noise in ultrasensitive signaling cascades. *Biophys J* 82:2943–50.

[3] Paulsson, J, Berg, OG, Ehrenberg, M (2000) Stochastic focusing: fluctuation-enhanced sensitivity of intracellular regulation. *Proc Natl Acad Sci USA* 97:7148–53.

[4] Elowitz, MB, Levine, AJ, Siggia, ED, Swain, PS (2002) Stochastic gene expression in a single cell. *Science* 297:1183–6.

[5] Ozbudak, EM, Thattai, M, Kurtser, I, Grossman, AD, van Oudenaarden, A (2002) Regulation of noise in the expression of a single gene. *Nat Genet* 31:69–73.

[6] Swain, PS, Elowitz, MB, Siggia, ED (2002) Intrinsic and extrinsic contributions to stochasticity in gene expression. *Proc Natl Acad Sci USA* 99:12795–800.

[7] Acar, M, Becskei, A, van Oudenaarden, A (2005) Enhancement of cellular memory by reducing stochastic transitions. *Nature* 435:228–32.

[8] Pedraza, JM, van Oudenaarden, A (2005) Noise propagation in gene networks. *Science* 307:1965–9.

[9] Thattai, M, van Oudenaarden, A (2001) Intrinsic noise in gene regulatory networks. *Proc Natl Acad Sci USA* 98:8614–9.

[10] van Zon, JS, Morelli, MJ, Tănase-Nicola, S, ten Wolde, PR (2006) Diffusion of transcription factors can drastically enhance the noise in gene expression. *Biophys J* 91:4350–67.

[11] van Zon, JS, ten Wolde, PR (2005) Green's-function reaction dynamics: a particle-based approach for simulating biochemical networks in time and space. *J Chem Phys* 123:234910.

[12] Allen, RJ, Warren, PB, ten Wolde, PR (2005) Sampling rare switching events in biochemical networks. *Phys Rev Lett* 94:18104.

[13] Macnamara, S, Burrage, K, Sidje, RB (2007) Multiscale modeling of chemical kinetics via the master equation. *Multiscale Model & Simul* 6:1146–1168.

[14] Ushikubo, T, Inoue, W, Yoda, M, Sasai, M (2006) Testing the transition state theory in stochastic dynamics of a genetic switch. *Chem Phys Lett* 430:139–43.

[15] Bortz, AB, Kalos, MH, Lebowitz, JL (1975) A new algorithm for Monte Carlo simulation of Ising spin systems. *J Comput Phys* 17:10–8.

[16] Gillespie, DT (1977) Exact stochastic simulation of coupled chemical reactions. *J Phys Chem* 81:2340–2361.

[17] Paulsson, J (2004) Summing up the noise in gene networks. *Nature* 427:415–8.

[18] Tănase-Nicola, S, Warren, PB, ten Wolde, PR (2006) Signal detection, modularity, and the correlation between extrinsic and intrinsic noise in biochemical networks. *Phys Rev Lett* 97:68102.

[19] Walczak, AM, Onuchic, JN, Wolynes, PG (2005) Absolute rate theories of epigenetic stability. *Proc Natl Acad Sci USA* 102:18926–31.

[20] Lan, Y, Papoian, GA (2006) The interplay between discrete noise and nonlinear chemical kinetics in a signal amplification cascade. *J Chem Phys* 125:154901.

[21] Lan, Y, Wolynes, PG, Papoian, GA (2006) A variational approach to the stochastic aspects of cellular signal transduction. *J Chem Phys* 125:124106.

[22] Lan, Y, Papoian, GA (2007) Stochastic resonant signaling in enzyme cascades. *Phys Rev Lett* 98:228301.

[23] Gomperts, BD, Kramer, IM, Tantham, PER (2002) Sig-

- nal transduction (San Diego, CA: Academic Press).
- [24] Ting, AY, Endy, D (2002) Decoding NF-kappaB signaling. *Science* 298:1189–90.
- [25] Detwiler, PB, Ramanathan, S, Sengupta, A, Shraiman, BI (2000) Engineering aspects of enzymatic signal transduction: photoreceptors in the retina. *Biophys J* 79:2801–17.
- [26] Bolouri, H, Davidson, EH (2003) Transcriptional regulatory cascades in development: initial rates, not steady state, determine network kinetics. *Proc Natl Acad Sci USA* 100:9371–6.
- [27] Bassler, BL (1999) How bacteria talk to each other: regulation of gene expression by quorum sensing. *Curr Opin Microbiol* 2:582–7.
- [28] van Kampen, NG (1992) *Stochastic processes in physics and chemistry* (Amsterdam: North-Holland).
- [29] Mattis, DC, Glasser, ML (1998) The uses of quantum field theory in diffusion-limited reactions. *Rev Mod Phys* 70:979–1001.
- [30] Zel'Dovich, YB, Ovchinnikov, AA (1978) The mass action law and the kinetics of chemical reactions with allowance for thermodynamic fluctuations of the density. *Sov JETP* 47:829.
- [31] Doi, M (1976) Second quantization representation for classical many-particle system. *J Phys A: Math Gen* 9:1465–77.
- [32] Sasai, M, Wolynes, PG (2003) Stochastic gene expression as a many-body problem. *Proc Natl Acad Sci USA* 100:2374–9.
- [33] Shannon, CE (1949) Communication in the presence of noise. *Proc IRE* 37:10–21.
- [34] Tkačik, G, Callan, CG, Bialek, W (2008) Information capacity of genetic regulatory elements. *Phys. Rev. E* 78:11910.
- [35] Tkacik, G, Callan, CG, Bialek, W (2008) Information flow and optimization in transcriptional regulation. *Proc Natl Acad Sci USA* 105:12265–70.
- [36] Cover, TM, Thomas, JA (1991) *Elements of Information Theory* (New York, NY: John Wiley and Sons).
- [37] Gregor, T, Tank, DW, Wieschaus, EF, Bialek, W (2007) Probing the limits to positional information. *Cell* 130:153–64.
- [38] Ziv, E, Nemenman, I, Wiggins, CH (2007) Optimal signal processing in small stochastic biochemical networks. *PLoS ONE* 2:e1077.
- [39] Lin, J (1991) Divergence measures based on the Shannon entropy. *Information Theory, IEEE Transactions on* 37:145–151.
- [40] A master equation in which the coordinate appears explicitly (e.g. through q_s or q_n in Eqn. 1) is sometimes mistakenly termed “nonlinear” in the literature, perhaps discouraging calculations which exploit its inherent linear algebraic structure. We remind the reader that this equation is perfectly linear.
- [41] The recursion can equivalently be performed in the reverse direction, with $g_N = 0$, $g_{N-1} = Np_N/p_{N-1}$, and $g_{n-1} = (g_n p_n + n p_n - (n+1)p_{n+1})/p_{n-1}$, where N is a cutoff in n . In several test cases we found that reverse recursion is more numerically stable than forward recursion at large N .
- [42] Setting $x = e^{ik_1}$ and $y = e^{ik_2}$ makes clear that the generating function is simply the Fourier transform.
- [43] $G(x, y)$ can be recovered by projecting onto position space $\langle x, y |$, with $\langle x | n \rangle = x^n$ and $\langle y | m \rangle = y^m$.
- [44] The adjoint operations are $\langle i | \hat{b}_i^+ = \langle i-1 | - \langle i |$ for $i \in \{n, m\}$, $\langle n | \hat{b}_n^-(n) = (n+1)\langle n+1 | - g_n \langle n |$, and $\langle n, m | \hat{b}_m^-(n) = (m+1)\langle n, m+1 | - q_n \langle n, m |$.
- [45] In position space the eigenfunctions are $\langle x | j \rangle = (x-1)^j e^{\bar{g}(x-1)}$ and $\langle y | k \rangle = (y-1)^k e^{\bar{q}(y-1)}$. The operators \hat{b}^+ and \bar{b}^- raise and lower in eigenspace: $\hat{b}_n^+ | j \rangle = | j+1 \rangle$ and $\bar{b}_n^- | j \rangle = j | j-1 \rangle$ (or $\langle j | \hat{b}_n^+ = \langle j-1 |$ and $\langle j | \bar{b}_n^- = (j+1) \langle j+1 |$), and similarly for $n \rightarrow m$ and $j \rightarrow k$.
- [46] The selection rules are derived by starting with $\langle n | \hat{b}_n^+ | j \rangle$ or $\langle j | \hat{b}_n^+ | n \rangle$ and allowing \hat{b}_n^+ to act both to the left and to the right. Alternatively, one may use \bar{b}_n^- , obtaining $\langle n+1 | j \rangle = (\langle j | n \rangle j - 1 + \bar{g} \langle n | j \rangle) / (n+1)$ and $\langle j+1 | n \rangle = (\langle n | j \rangle n - 1 - \bar{g} \langle j | n \rangle) / (j+1)$, initialized with $\langle n=0 | j \rangle = (-1)^j e^{-\bar{g}}$ and $\langle j=0 | n \rangle = 1$. We find the latter relations yield smoother distributions p_{nm} for large cutoffs N and J .
- [47] The choices of \bar{g} and \bar{q} can affect the numerical stability of the method, as will be discussed in future work.
- [48] More precisely, we have turned an $N^2 \times N^2$ matrix solve (where N is a cutoff in copy count) into K length- J vector solves (where J and K are cutoffs in eigenmodes j and k respectively).
- [49] All numerical procedures in the paper are implemented in MATLAB.
- [50] Although the spectral method only involves the calculation of joint distributions between adjacent species in the cascade, the input-output distribution can be obtained using $p(n_1, n_\ell) = \sum_{n_{\ell-1}} p(n_1, n_{\ell-1}) p(n_{\ell-1}, n_\ell) / p(n_{\ell-1})$, initialized with $\ell = 3$ and run up to $\ell = L$. This assumes $p(n_1 | n_{\ell-1}, n_\ell) = p(n_1 | n_{\ell-1})$, which at worst (at $\ell = 3$) is equivalent to the Markovian approximation, Eqn. 2.
- [51] There is a slight decrease in I^* with $\langle n \rangle$ beginning near $\langle n \rangle \approx 8$ that is more pronounced at higher L . This is likely due to the decrease in accuracy of the Markovian approximation with increasing Δ (cf. *Supplementary Material*), since large $\langle n \rangle$ requires large Δ . Calculations with the full joint distribution (via stochastic simulation) at $L = 3$ and 4 give qualitatively similar results, but with I^* increasing monotonically with $\langle n \rangle$.
- [52] The decrease of I^* with L is consistent with, but not a direct consequence of, the data processing inequality [36], as each $p^*(n_1, \dots, n_L)$ results from a separate optimization for each subsequent choice of L .